Article

Influence of Central Air on Flow and Combustion Characteristics and Low-Load Stabilization Performance of a Babcock Burner

Chunchao Huang [1], Zhengqi Li [1,*], Yufei Wang [1], Yue Lu [1], Huacai Liu [2] and Zhichao Chen [1]

[1] School of Energy Science and Engineering, Harbin Institute of Technology, 92, West Dazhi Street, Harbin 150001, China; ustbhuangchunchao@163.com (C.H.); wangyufei717@163.com (Y.W.); luyue90@163.com (Y.L.); chenzc@hit.edu.cn (Z.C.)

[2] Guangzhou Institute of Energy Conversion, Chinese Academy of Sciences, 2, Nengyuan Rd., Wushan, Tianhe District, Guangzhou 510640, China; liuhc@ms.gies.ac.cn

* Correspondence: green@hit.edu.cn; Tel.: +86-135-0362-1484

Abstract: On a cold single-phase test stand, the effect of central air on the exit flow field of Babcock, Germany, burner was investigated. Industrial measurements were taken for a 700 MW wall-fired pulverized-coal utility boiler with above burners. Gas temperature, gas composition and concentration in the burner area were measured at 444 MW, 522 MW and 645 MW loads, respectively. Only when the central air mass flow was zero did a center reflux zone exist in the burner outlet area. The steady combustion of faulty coal was aided by early mixing of primary and secondary air, which was made possible by the decreased central air mass flow. At all different loads, the pulverized coal in center region took a long distance to ignite. The temperature in center steadily dropped as central air mass flow decreased, while the temperature in secondary air region gradually rose. Within 1.5 m from the primary air duct outlet, the highest CO concentration was 25 ppm and the highest O_2 concentration was close to 21% under all loads. The gas concentration near sidewall was more influenced by load. With all valves opening of burner center air at 30%, the boiler was able to operate safely and stably without oil at a load of 262 MW. The furnace chamber temperature in burner area reached 1056.1 °C.

Keywords: swirl burner; central air; flow characteristics; low-load stable combustion

1. Introduction

In order to cope with atmospheric pollution [1,2] and the greenhouse effect [3], the Chinese government has proposed the goal of carbon peaking and carbon neutrality. It provides a good opportunity for the development of new energy, such as photovoltaic power and wind power. According to statistics for the electricity industry issued by the China National Energy Administration for January to February 2023, the installed wind power capacity climbed by 11.0%, while the installed photovoltaic power capacity increased by 30.8% year over year [4]. However, new energy such as wind and photovoltaic are intermittent, volatile and stochastic in nature [5]. New energy generation grows and needs to temper the massive oscillations of scaled photovoltaic and wind power. The necessity for thermal power units to cycle through peak loads in depth will become the new normal. In order to meet the requirements of deep peak regulation, coal-fired boilers must have a minimum technical output of 30% of their rated capacity or even less, and taking into account low nitrogen oxide (NO_x) emissions [4]. China is one of the few countries in the world having abundant reserves of anthracite and lean coal. Anthracite and lean coal make up 11.5% and 5.5%, respectively, of China's proven coal reserves; both coals make up more than 40% of the coal used in domestic coal-fired utility boilers [6]. However, the lean coal-fired boilers in China can currently only work at a minimum stable combustion rated load of roughly 50%, which does not meet the requirements of deep peak regulation.

The swirling combustion system exhibits a significant advantage over the tangentially fired boiler in terms of slagging and temperature deviation [7]. The majority of large-scale units in Europe and America adopt swirling combustion systems. The foreign swirl combustion technology is relatively mature, and few improvements have been made in recent years. Most of the domestic swirl combustion technology is imported from abroad. More than 40% of domestic coal-fired facilities with loads of 300 MW and above use swirl pulverized coal burners [8]. Practically speaking, the majority of swirl burners, including LNASB burner [9], IHI dual swirl burner [10], and HT-NR3 burner [11,12], are set up with central air. The central air has two purposes: first, it provides air that the ignition system needs; second, it cools the ignition equipment. In addition, the central air is also one of the important regulating means for swirl burners [13]. Wang et al. [14] conducted a gas-solid two-phase test using Phase Doppler anemometry (PDA). Their findings demonstrated that the central air was able to regulate the distribution of coal powder, and could further to optimize combustion and prevent nozzle slagging. In the case of swirl combustion, Lu et al. [15] used Particle Image Velocimetry (PIV) to investigate the effect of central air on air flow structure. They discovered that a larger central air flow might significantly enhanced the mixing of fuel and air. For a certain equivalence ratio, Huang et al. [16] showed that the inclusion of central air could improve the flame stability and optimize the flame shape. In addition, several studies had demonstrated that increasing the central air in a swirl burner could effectively decrease the emissions of NO_x [17–19]. For example, Xie et al. [20] investigated the effect of secondary air flaring angle and central air ratio on NO_x emissions of HT-NR3 burner, using a thermal test stand. It is clear that the current domestic study mainly focused on how central air influenced NO_x emission and nozzle slagging. Moreover, the majority of the study techniques used laboratory tests and numerical simulations. There were few industrial tests on the ability of central air for regulating and stabilizing low-load combustion.

Many studies have been conducted abroad for boilers low-load stabilization. To increase the flexibility of plants, Marcel et al. [21] inserted steam accumulators, often referred to as Ruths storage, into power plants. According to Martin et al. [22], the cooperative control system (CCS) of thermal power plants could be optimized to enhance the peak load regulation capacity of coal-fired units. Foreign research is mainly focused on improving detection and control systems, with little emphasis on burner optimization. Compared to the high cost of optimizing the system, the burner retrofit is less expensive, with low degree of operation difficulty.

This study aimed to determine how central air affected the gas flow and thermal combustion performance of a Babcock burner, and to further investigated the role of central air in regulating the low-load stable combustion. In this work, a single swirl burner model at laboratory scale was developed with a size ratio of 1:5.5 to full-sized burner. Then, a cold experimental system for single-phase testing was constructed using above model. Utilizing thin cloth and constant temperature anemometer (IFA 300), the flow direction and velocity of burner outlet were measured. Based on the result of single-phase test, the optimal central air mass flow was obtained. In addition, industrial tests were conducted on a 700 MW boiler equipped with the aforementioned burners. Lean coal was served as the primary fuel source. At 645 MW (92.1% rated load), 522 MW (74.6% rated load) and 444 MW (63.4% rated load), respectively, the effects of central air on gas temperature, gas type and concentration were studied. Further, a stable combustion test was performed at 280 MW (40.0% rated load) and 262 MW (37.4% rated load). The results obtained in this study provided experimental data for further numerical simulation studies and suggested a potential route for increasing the flexibility of this type of boiler. Moreover, it served as an exploration of the fine-tuning operation of boilers powered by low-quality coal, aiming to enhance their stable combustion capability at low loads.

2. Utility Boiler

The 700 MW unit boiler was manufactured by Babcock, Germany. The boiler is a subcritical natural circulation drum boiler with solid-state slagging. The burners of this boiler are arranged on both front and rear walls, however, burners on the same level are not located at the same elevation. More specifically, the front wall burner is located 2.125 m higher than the rear wall burner, at the same layer. The burners are arranged in 3 layers on each of the front and rear wall, 4 on each layer, for a total of 24 burners. The over fire air (OFA) burners are arranged on top of the upper layer of burners, with 2 rows of 8 burners each on the front and rear wall, for a total of 32 OFA burners. Layout of the furnace and combustion device is shown in Figure 1. Five double-ended ball mills and a positive-pressure direct-fired system are used to supply pulverized coal to the burners. The boiler is fueled by a mixture of lean coal and bituminous coal.
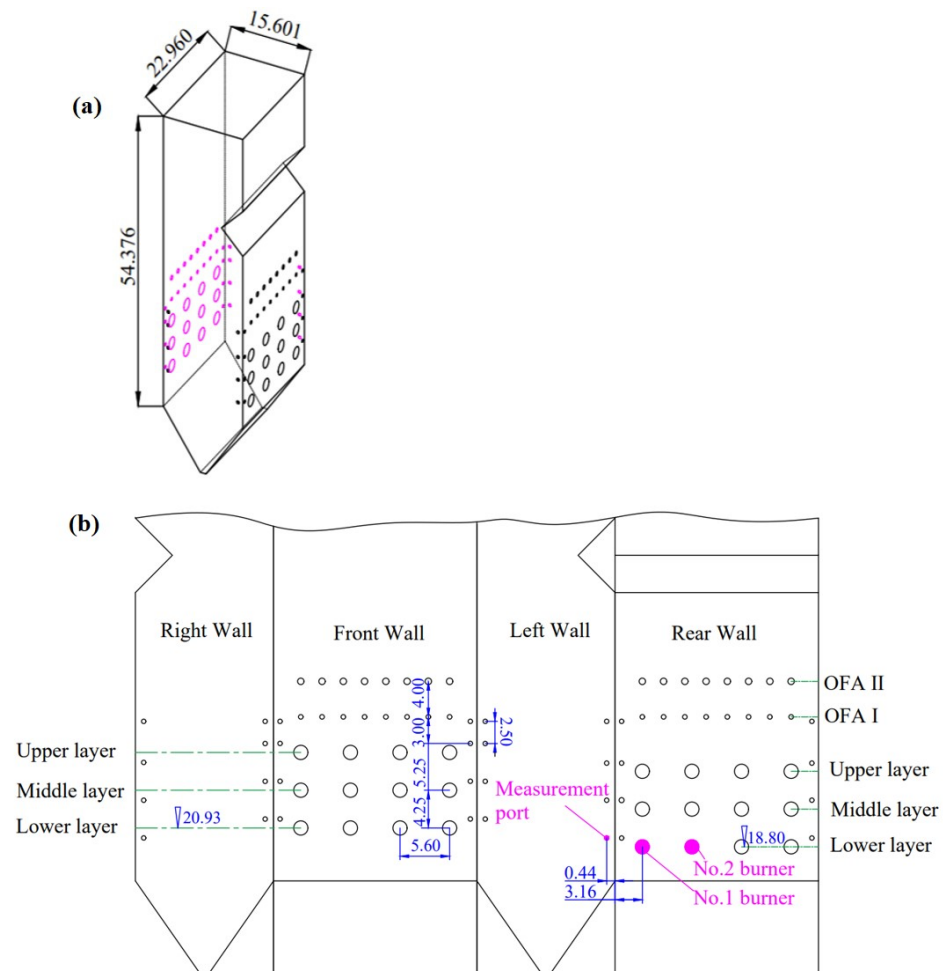
Figure 1. Arrangement of furnace and combustion equipment (unit: m): (**a**) Three-dimensional structure of the furnace, (**b**) Unfolded diagram of the furnace.

Figure 2 shows the burner structure. After passing through the volute, the secondary air is divided into rotating inner and outer secondary air. Subsequently, the inner and outer secondary air pass through their respective axial blades. To effectively control the swirling intensity of secondary air, one can adjust the position of volute inlet baffle and the axial blades angles. The primary air duct is situated at burner center, allowing the primary air to flow through the axial blades. By adjusting the angle of primary air blades, the swirling intensity of primary air can be modified. The air duct that provides straight-flow central air is installed inside the primary air duct. In practical operation, the inner and outer secondary

air blades are both set at 45° in relation to the center axis of burner, while the primary air blades are positioned at 30°. The burner design parameters are shown in Table 1.
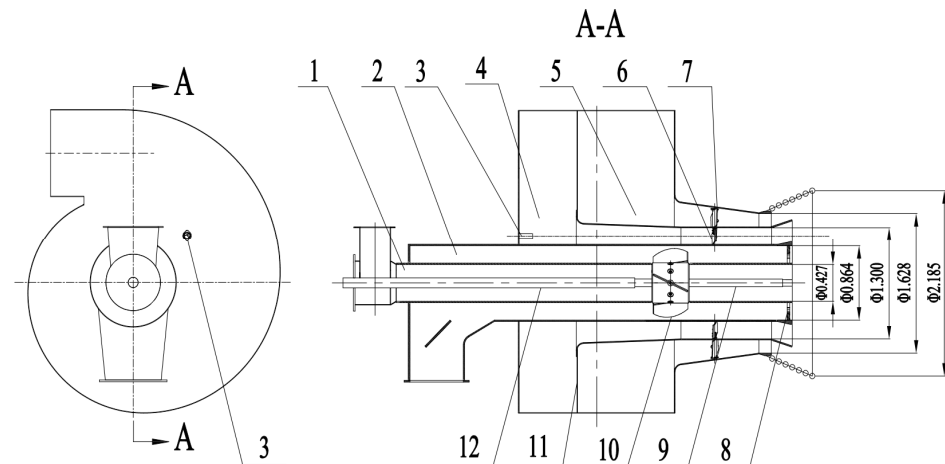
Figure 2. Burner structure diagram (unit: m): (1) central air duct, (2) primary air duct, (3) Monitoring port, (4) volute of inner secondary air, (5) volute of outer secondary air, (6) axial blades of inner secondary air, (7) axial blades of outer secondary air, (8) flame stabilizing ring, (9) oil gun, (10) axial blades of primary air, (11) volute partition board, (12) oil gun sleeve.

Table 1. Burner design parameters.

Items	Parameters
Passage area of the primary air (m^2)	0.4221
Exit area of the primary air (m^2)	0.2754
Exit area of the inner secondary air (m^2)	0.8608
Exit area of the outer secondary air (m^2)	0.8251
Exit area of the central air (m^2)	0.1431
Temperature of the primary air (°C)	119
Temperature of the secondary air (°C)	325
Mass flow rate of the primary air (kg·s^{-1})	6.67
Mass flow rate of the inner secondary air (kg·s^{-1})	5.47
Mass flow rate of the outlet secondary air (kg·s^{-1})	7.21
Mass flow rate of the central air (kg·s^{-1})	1.83

3. Cold Air Experiments of the Burner Model

3.1. Test Instruments and Methods

3.1.1. Single-Phase Experimental Equipment

Based on the theory of isothermal modeling [23], a testing system was constructed to model the cold-state of a single burner (scaled down by a factor of 5.5). The experiment system is illustrated in Figure 3. The variable *x* denotes the distance from burner exit, while r represents the distance from burner center axis. To conduct experiments, different devices should be selected to measure.

3.1.2. Single-Phase Experimental Method

(1) The airflow spread angle and the boundary of recirculation zone were measured by using a coordinate frame with thin cloth. The distance between adjacent grids is 0.05 m. The boundary of jet and recirculation zone are determined according to the direction of thin cloth [24]. To obtain the boundary of recirculation zone, the farthest point that points towards the burner outlet is connected. This boundary line divides the flow field into two regions: the mainstream zone outside the boundary and the recirculation zone inside it. To determine the airflow spread angle, the following conditions must be met: the thin cloth must remain stationary and be positioned closest to the central axis. The boundary line is

formed by connecting the obtained points. The angle between this boundary line and the central axis is defined as the airflow spread angle.
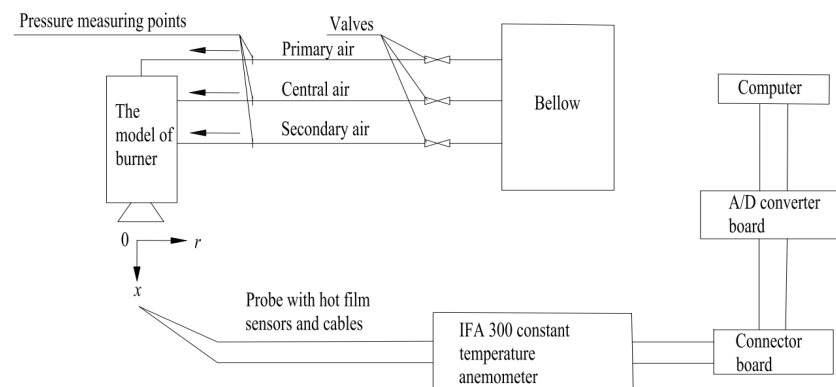
Figure 3. Experimental system for cold model.

(2) The velocities of air flow at various cross sections of the burner outlet, including axial, tangential, and radial velocity, were measured using a constant temperature anemometer (IFA300). According to the reference [25], the velocity measurement error of IFA300 is less than 5%. The velocity boundary point is defined as the position point that is closest to the burner center axis, with zero axial velocity. The velocity boundary line is then obtained by connecting these velocity boundary points. The axial velocity inside the boundary line is negative, while outside the boundary line is positive. Additionally, the average value of the absolute axial velocity is calculated, and 10% of the average value is considered as the minimum axial velocity. In order to obtain the airflow spread angle, a boundary line is formed by connecting the position points corresponding to the minimum axial velocity at each cross section. The angle between it and the center axis is defined as the airflow spread angle measured by IFA300.

3.1.3. Single-Phase Experimental Parameters

Based on the parameters of full-scale burner, the experimental parameters of model burner under normal temperature conditions are obtained, as shown in Table 2. The condition with central air mass flow of 0.112 kg·s^{-1} is taken as the reference condition.

Table 2. Experimental parameters at different central air mass flow under cold conditions.

Central Air Mass Flow to Reference Condition (%)	Central Air Mass Flow (kg·s^{-1})	Inner Secondary Air Mass Flow (kg·s^{-1})	Outer Secondary Air Mass Flow (kg·s^{-1})	Primary Air Mass Flow (kg·s^{-1})	Airflow Spread Angle Measured by Thin Cloth (°)
0	0	0.337	0.444	0.393	46
30	0.033	0.337	0.444	0.393	43
60	0.067	0.337	0.444	0.393	40
100	0.112	0.337	0.444	0.393	32
130	0.145	0.337	0.444	0.393	28

3.2. Result of Cold Air Experiments

3.2.1. Jet Boundary and Recirculation Zone Boundary of Burner under Different Central Air Mass Flow

The spread angles under different central air flow, as measured by thin cloth, are presented in Table 2. While the central air flow decreases from 130% to 0%, the spread angle of jet boundary increases gradually from 28° to 46°. The spread angles are relatively close when the center air flows are 0%, 30% and 60%. The mass flows of inner secondary air, outer secondary air, as well as the primary air, remain constant under different operating

conditions. Therefore, with the increase of center air mass flow, the overall jet axial momentum at burner outlet also increases, resulting in a decrease in the spread angle.

The jet boundary, recirculation zone boundary, and velocity boundary under different central air flows, measured by the thin cloth, are shown in Figure 4. x refers to the distance along the jet direction to burner outlet; r represents the distance along the radial direction to the burner center axis; d is the diameter of the burner outlet (d = 0.375 m). According to Figure 4, the recirculation zone only appears when the center air mass flow is 0%. A small center recirculation zone near the central air duct is attributed to the blunt body effect. The significant center recirculation zone along the centerline between x/d = 1.07–1.87 is attributed to the entrainment of secondary air. However, the coal concentration in burner central area is small because of the swirling primary air. At the same time, the large recirculation zone is located far away from the burner outlet. Based upon the interaction of all of two factors., the large recirculation zone has minimal impact on stable combustion of pulverized coal.
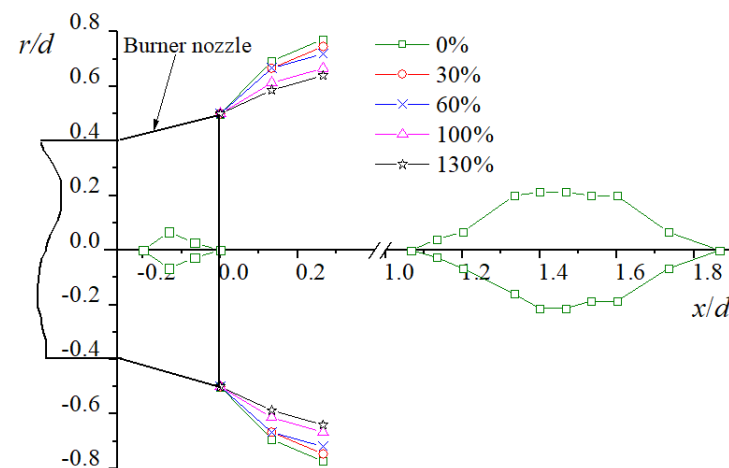
Figure 4. Jet boundary and recirculation zone boundary measured by thin cloth.

Figure 5 displays the velocity boundary points obtained by using IFA300. It can be seen that under different central air mass flows, there are annular velocity boundaries near r/d = 0.2–0.45 in x/d = 0–0.25 s. Furthermore, all velocity boundary lines exhibit similar sizes and shapes. The formation of annular velocity boundaries is mainly influenced by the flame stabilizing ring. The stabilizing ring acts as a blunt body, which results in a lower local pressure behind it, causing the airflow to flow back. Thus, the axial velocity inside the velocity boundary line is negative. However, due to its relatively low height, it can be difficult to pinpoint the boundary of the annular recirculation zone when employing thin cloth for measurement. Meanwhile, Figure 5 also indicates that in the absence of central air, a central velocity boundary exists between x/d = 1.0 to x/d = 2.0. The presence of this zone is shown by the fact that the axial velocity inside the boundary is less than 0. When the central air flow is more than 0, the negative pressure state at burner center is disrupted, thereby impeding the formation of a stable central recirculation zone. Compared to Figure 4, Figure 5 shows a larger central recirculation zone. The primary cause for this phenomenon is the mass of thin cloth, which necessitates a certain airflow velocity to drive it. Consequently, the central recirculation zone, as measured by the thin cloth, is relatively small.
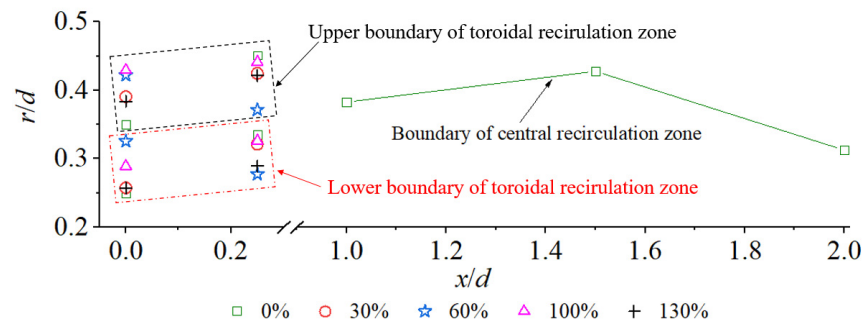
Figure 5. Velocity boundary measured by IFA300.

The jet boundary measured using IFA300 is detailed in Figure 6. When the central air mass flow is 0%, 30%, 60%, 100% and 130%, the corresponding jet spread angles is 34°, 30°, 26°, 25° and 20°, respectively. The central air is straight wind, and the axial momentum increases with the increase of its mass flow. As a result, the spread angle value gradually diminishes. This, in turn, suggests that a greater mass flow of central air is detrimental to the diffusion and mixing.
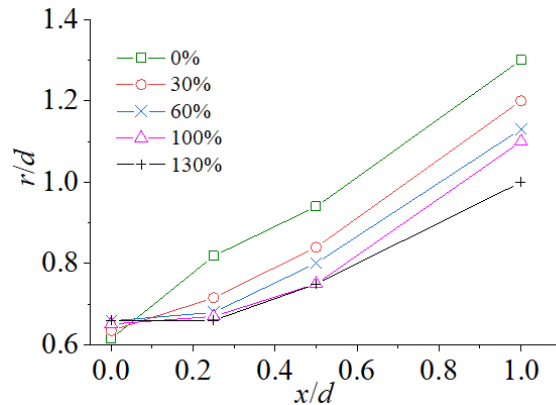
Figure 6. Jet boundary measured by IFA300.

The role of the central air is mainly to regulate the recirculation zone. However, from the results of Figure 4, for 30% to 130% of the central air mass flow, there is no recirculation zone at the burner outlet. Meanwhile, the results in Figure 5 reveal that the formation of the toroidal recirculation zone is mainly dependent on the flame stabilizing ring. These demonstrate that for this burner, the central air does not play a role in regulating combustion. Moreover, the primary air of this burner is whirlwind and has a large radial velocity (see Figure 9). In practical use, the coal powder is primarily spread to the wall region far from the burner center because it is strongly transported along the radial direction. Due to the early entry of a substantial amount of coal powder into the low temperature secondary air zone, ignition and stable combustion are not possible. Therefore, the burner has poor combustion stabilization performance.

3.2.2. Speed Distribution of Burner with Different Central Air Mass Flow

Figure 7 demonstrates the average axial velocity distribution under different central air mass flow. In the figure, d represents the diameter of burner outlet, where d = 0.375 m. There are two peaks in the axial velocity along the radial direction, ranging from $x/d = 0$ to $x/d = 0.5$. The peak closer to the center is formed by the primary air, while the peak further away from the center is formed by the secondary air. As the airflow develops, the peak representing the secondary air gradually decreases while also moving away from the burner center. The burner is operated with a large primary air velocity. In $x/d = 0$–0.25 s, the velocity distribution of central area is mainly influenced by the primary air. After the

primary air is gradually mixed with the secondary air, the irrotational central air still has a strong penetration. Therefore, after x/d = 0.5 s, the axial velocity distribution in the central region is significantly affected by the central air. Compared to other central air mass flows, the axial velocity distribution is significantly different when the central air mass flow is either 0% or 30%. When the central air mass flow is 0%, a low-speed zone appears in r/d = 0–0.2. Similarly, when the central air mass flow is 30%, there is also a low speed zone in r/d = 0.25–0.45. In x/d = 1.0–2.0 s, the axial velocity close to the burner center steadily reduces as the central air mass flow diminishes. It is worth noting that the central duct is equivalent to a blunt body when central air mass flow is 0%. As depicted in Figure 4, the axial velocity is less than 0 within the range of r/d = 0 to r/d = 0.35, indicating the formation of a recirculation zone. Apart from the condition without central air, the axial velocity is also notably lower at 30% mass flow. For this type of burner, the use of a smaller central air mass flow can effectively reduce the axial velocity in burner central region, which is more conducive to strengthen the mixing of secondary air and primary air. It is beneficial to the ignition of fault coal.
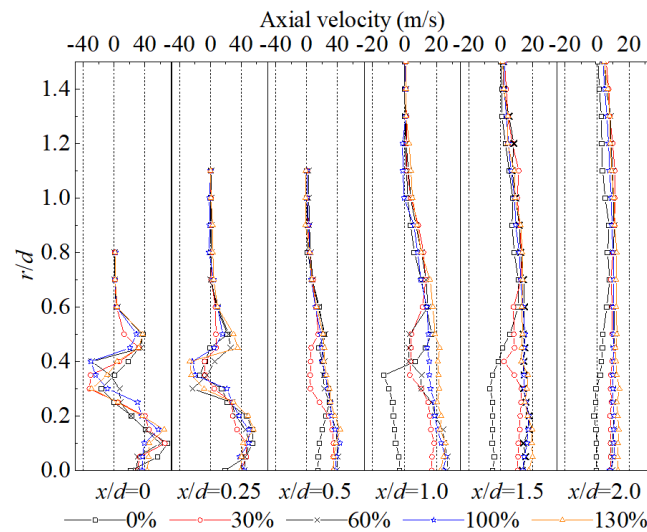
Figure 7. Axial average velocity distribution under different central air mass flow.

The recirculation zone entrains high temperature flue gas, thus providing the necessary heat for igniting pulverized coal. Therefore, the stable combustion of swirl burner mainly depends on the size of recirculation zone and the net return flow of flue gas. In Figure 5, the boundary line of annular recirculation zone is considered to be the region formed by the velocity boundary points within x/d = 0–0.25. As the annular recirculation zone is symmetrical, the length and maximum diameter of the half annular recirculation zone are denoted by L and D, respectively. Since the IFA300 requires the selection of a specific cross-section for measurement, the L remains constant at 0.25d for all operating conditions. In addition, the positive flow ratio (q_{r+}) and negative flow ratio (q_{r-}) are introduced under the same cross-section. q_{r-} is the ratio of the axial recirculation volume flow in the recirculation zone to the primary air volume flow; q_{r+} is the ratio of the axial positive volume flow outside the recirculation zone (near the burner central axis) to the primary air volume flow. The calculation formula is:

$$q_{r-} = \frac{\int_{R_1}^{R_2} 2\pi u r dr}{Q_1} \tag{1}$$

$$q_{r+} = \frac{\int_{0}^{R_1} 2\pi u r dr}{Q_1} \tag{2}$$

wherein u is the axial velocity on the measured cross-section, $m \cdot s^{-1}$; R_1 and R_2 respectively denote the initial and final radius of the recirculation zone, $R_2 < 0.45d$, m; Q_1 stands for the primary air volume flow, $m^3 \cdot s^{-1}$.

Table 3 reflected the recirculation zone size and flow ratio, where the net flow ratio $\Sigma q = (q_{r+}) - (q_{r-})$. The stabilizing ring has a major impact on the formation of annular recirculation zone, so the D does not greatly change depending on the operating conditions. The central air has no discernible effect on q_{r-} and q_{r+} at $x/d = 0$ and $x/d = 0.25$, whereas the net flow ratio Σq shows a high association with the central air mass flow. Overall, Σq is positive across different central air mass flow and grows progressively with rising central air mass flow. Thus, it can be concluded that within $x/d = 0–0.25$, the central region of burner is dominated by the outflow of air. A reduced central air mass flow, however, can actually reduce the net mass flow ratio and improve flue gas recirculation in center of the entire burner outlet.

Table 3. Recirculation zone size and mass flow ratio.

Parameter	Central Air Mass Flow				
	0%	**30%**	**60%**	**100%**	**130%**
D/d	0.13	0.13	0.11	0.14	0.13
q_{r+} (x/d = 0)	3.04	3.23	3.53	4.19	3.95
q_{r-} (x/d = 0)	1.52	1.70	1.37	1.85	1.58
Σq (x/d = 0)	1.52	1.53	2.16	2.34	2.37
q_{r+} (x/d = 0.25)	3.03	3.15	3.84	4.97	5.60
q_{r-} (x/d = 0.25)	0.95	0.59	0.91	2.06	2.59
Σq (x/d = 0.25)	2.08	2.56	2.93	2.91	3.01

Figure 8 illustrates the distribution of tangential average velocity for various central air mass flow. The tangential velocity in the radial direction displays two peaks at the range of $x/d = 0–1.0$. The peak near the center (about $r/d = 0.2$) is produced by the primary air, while the peak distant from the center (around $r/d = 0.5$) is produced by the secondary air. As the flow keeps going, these two peaks progressively merge into a single peak at $x/d = 1.5$. The air flow near the burner outlet axis ($r/d = 0–0.15$) has zero tangential velocity at the range of $x/d = 0–0.25$. This is mainly due to the uneven radial velocity distribution of the rotating primary air, resulting in a weaker rotation in center. It is further shown that the central air has little effect on the tangential velocity in the above range. After $x/d = 0.5$, the central air is gradually carried by the rotating primary air, resulting in rotation. However, the starting section of the central air rotation is related to its own mass flow. In addition, the primary air shows a weak rotation at the center and an unequal velocity distribution in the radial direction. The modification in central air mass flow significantly affects the tangential velocity at center of the burner within $x/d = 0.5–1.0$. The region of zero tangential velocity falls to $r/d = 0–0.05$, when the central air mass flow is reduced to 30% and 0%. At the section where $x/d = 1.5–2.0$, the degradation of tangential velocity in that area accelerates with the decrease of central air mass flow. According to the research results of Wang et al. [14], it can be extrapolated that the addition of central air can increase the rigidity of rotating primary air and postpone the mixing of primary and secondary air. The early interaction between coal and secondary air is thereby facilitated by adopting a lower central air mass flow, increasing combustion stability. Therefore, using a smaller central air mass flow is beneficial for enhancing stable combustion.

The radial average velocity distribution for various central air mass flow is indicated in Figure 9. The radial velocity has two peaks on the section of $x/d = 0$ to $x/d = 0.5$. The primary air is what causes the peak at $r/d = 0.25$, while the secondary air is what causes the peak at $r/d = 0.5$. The two radial velocity maxima eventually deviate from the burner centerline due to the diffusion of primary and secondary air. The two peaks merge into one when the airflow reaches $x/d = 0.5$, demonstrating that the two airflows have been

merged. The five working circumstances, in particular, can create a negative radial velocity in the range of r/d = 0.20–0.40 (x/d = 0–0.25), suggesting that the air flow in this region is moving in the direction of burner centerline. While the airflow shifts to x/d = 0.5, the mass flow of central air also significantly affects the radial velocity distribution in the burner central zone. Within the range of x/d = 1.0–1.5, the radial velocity of r/d = 0–0.5 decreases with the reduction in the center air mass flow.
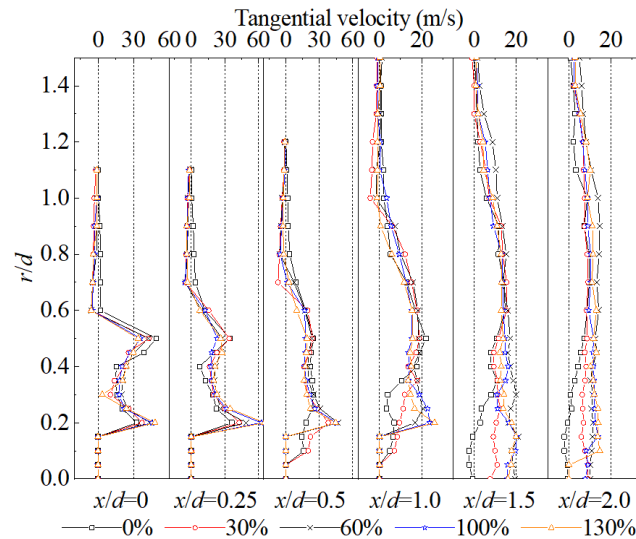
Figure 8. Tangential average velocity distribution under different central air mass flow.
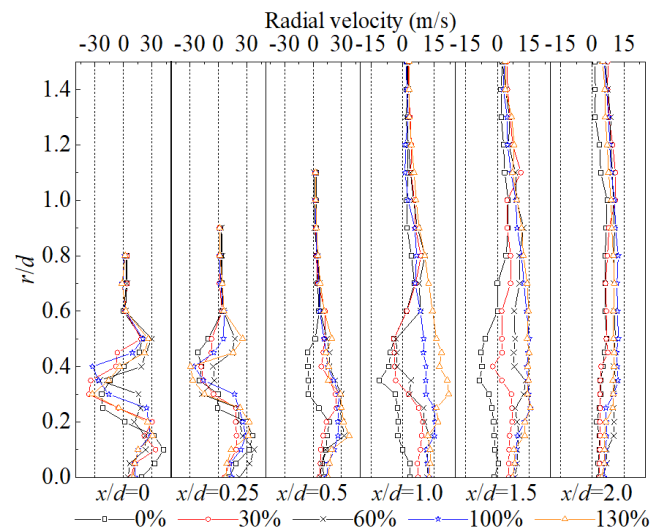
Figure 9. Radial average velocity distribution under different central air mass flow.

Figure 10 illustrates the position of maximum axial positive velocity for different central air mass flow. The highest axial velocity peak divides into two at x/d = 0 and x/d = 0.25, which correspond to the peaks of primary air velocity (near r/d = 0.10–0.15) and secondary air velocity (near r/d = 0.45–0.5), respectively. The peak position in the first two sections is not significantly affected by the central air. The axial velocity peaks merge as the primary and secondary air gradually converge to x/d = 0.5. As the central air mass flow drops, the peak position under the same cross section gradually moves farther from the burner centerline. According to this, the mixing of primary air and secondary air is advanced. Thus, the diffusion ability of airflow is higher at a lower central air mass flow, further contributing to the steady combustion of low-quality coal. Additionally, the peak at x/d = 0.5–1.0 with 30%, 60%, 100% and 130% central air mass flow are successively

clustered around r/d = 0.1. When the airflow moves to x/d = 1.5–2.0, the peak position of r/d gradually increases with the decrease of central air mass flow. In this case, compared to other conditions, the r/d values of 0% and 30% mass flows are significantly larger. The primary cause of the aforementioned occurrence is that while the central air mass flow drops, the axial momentum of outlet airflow also diminishes, thereby enhancing its ability to diffuse substances more efficiently.
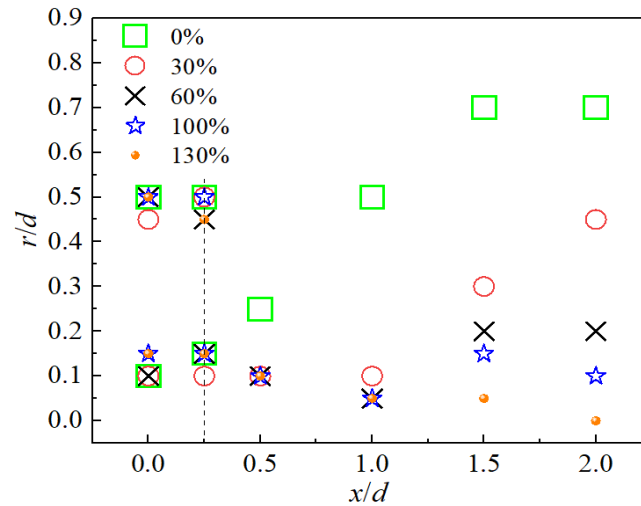
Figure 10. Position of maximum axial positive velocity.

Figure 11 presents the position of maximum tangential velocity at different central air mass flow. There are two tangential velocity peaks at x/d = 0 and x/d = 0.5, one near r/d = 0.2 and the other near r/d = 0.5, corresponding to the maximum velocity of primary air and secondary air, respectively. In the cross-section of x/d = 0–0.5, the impact of central air on peak position of primary and secondary air is not immediately apparent. The rotating primary and secondary air eventually mix as the airflow moves to x/d = 1.0. Then, the two tangential velocity peaks combine to form a single peak. The x/d = 1.0–2.0 s make it evident that the position of maximum tangential velocity is always in the secondary air area (r/d = 0.5), even though the central air mass flow is 0% and 30%. While the central air mass flow is 60%, 100% or 130%, the maximum tangential velocity is focused mostly in the burner center (r/d = 0–0.25). This is because with the increase of central air mass flow, the axial momentum of airflow increases. It destroys the mixing of primary air and secondary air, making the primary air still maintain a strong rotation after x/d = 1.0. It can also be concluded that only until the airflow reaches x/d = 1.0 will the change in central air mass flow have a significant effect on the tangential velocity. Furthermore, the decreased central air mass flow facilitates the dispersion of swirling primary air in the radial direction, enhancing the amalgamation of primary and secondary air, and further expediting the combustion of pulverized coal.

Figure 12 illustrates the variation in turbulence intensity at different central air mass flow. The turbulence intensity T is defined as [26]:

$$T = \sqrt{\frac{1}{3}(\overline{U'^2} + \overline{V'^2} + \overline{W'^2})}/U_0 \qquad (3)$$

In Equation (3), $\overline{U'^2}$, $\overline{V'^2}$ and $\overline{W'^2}$ represent the fluctuation values of axial, radial, and tangential velocities, respectively. The symbol U_0 represents the mean velocity. According to Figure 12, the distribution of turbulence intensity is non-uniform, with lower turbulence intensity observed at both the jet boundary and the central axis. On the cross-section from x/d = 0 to x/d = 0.25, T exhibits a bimodal distribution, with peaks occurring at approximately r/d = 0.1 and r/d = 0.35. With the development of airflow, these two peaks

decay rapidly. The mixture of the non-rotating central air and the rotational primary air causes the peak near r/d = 0.1, and the mixture of inner and outer secondary air causes the peak near r/d = 0.35. The T distribution at the burner outlet has a great influence on the combustion process. As the central air mass flow diminishes in the early stages of airflow (x/d = 0 to x/d = 0.25), the level of turbulence gradually increases around r/d = 0.1, increasing the degree of airflow mixing and promoting the premature combustion of coal. While the central air mass flow rises from 30% to 130%, The turbulence intensity around burner center steadily increases at x/d = 0.5 to x/d = 1.5. Specifically, it can be seen from Figure 4 that due to the presence of a central recirculation zone at x/d = 1.0 to x/d = 1.87, a high airflow mixing effect is produced, when the central air mass flow is zero. Therefore, for the cross-section of x/d = 1.0 to x/d = 1.5 at Figure 12, the turbulence intensity is rather significant. It can be seen that while the central air mass flow is 0–30%, it is favorable for the mixing of each air flow.
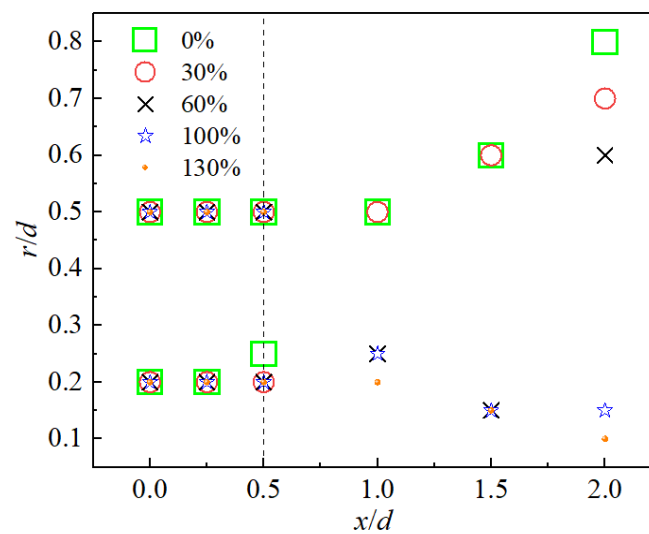
Figure 11. Position of maximum tangential velocity.
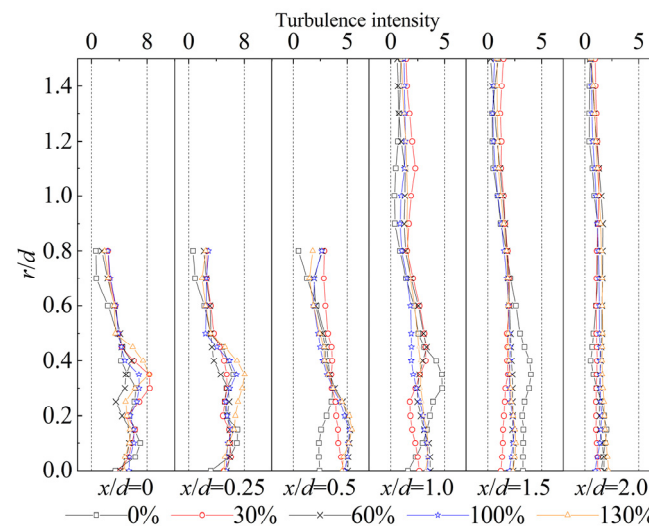
Figure 12. Distribution of turbulence intensity under different central air mass flow.

4. Industrial Measurement of Burner and Boiler Low Load Operation Experiment

4.1. Data Acquisition Techniques

Swirl burners operate independently and that temperature and velocity field of each differ only slightly. Therefore, the combustion performance of this type of burner can be

determined by measuring one burner. Figure 13 displays the bottom swirl burner on the rear wall from top-view. Burner No. 2 in this layer was selected to function as the gas temperature, species, and concentration for the burner outlet. Burner No. 1 in this layer was selected to monitor the gas species and concentration in the radial direction.

(1) Measurement of the gas species and concentration in the central axis of burner.

In order to measure the species and concentration of gas. the oil gun in the burner center should be removed. A water-cooled stainless steel probe was then put into the burner outlet area (as shown in Figure 13) through the oil gun sleeve (as depicted in Figure 2). The measurement starting point (X = 0) is on the outlet of primary air duct. The water-cooled probe has a total length of 6.9 m and a measurement range of 0 to 1.5 m. The water-cooled section structure of the probe can be seen in Figure 14. The extracted gases were analyzed online using a Testo-350M flue gas analyzer. The measurement error of the Testo-350M was 0.2% for O_2 concentration and 5% for CO and NO_x concentrations [27]. The sensor module has been calibrated before the test.

(2) Measurement of the gas species and concentration in the radial direction of burner.

Figure 15 illustrates the position of measurement port on left wall. In order to measure the gas species and concentration in the radial direction of burner No. 1, the water-cooled stainless steel probe is inserted along the measurement line. The measuring approach is identical to that mentioned in (1). The left water-cooled wall serves as the reference point, and the test range is from 0 to 1.5 m. The elevation of burner and the distance between measurement port and front wall are illustrated in Figure 1.
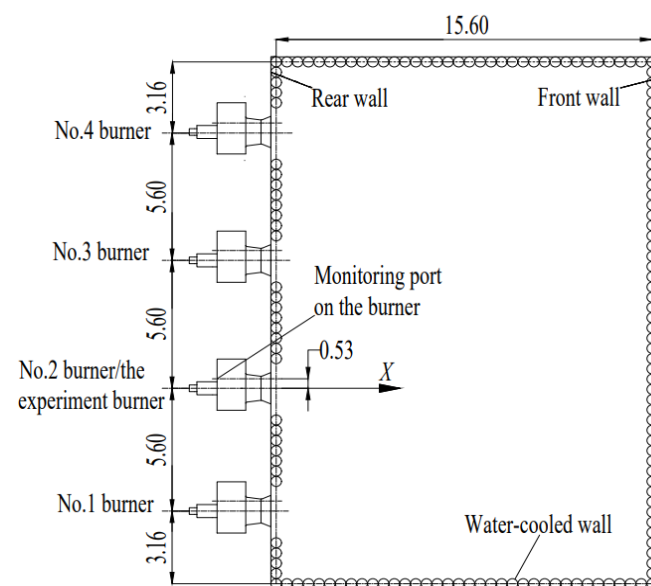
Figure 13. Top view of burners on the rear wall (unit: m).
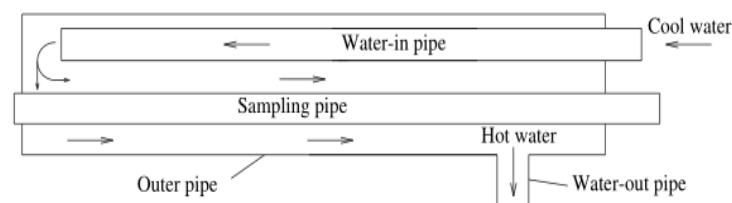
Figure 14. The water-cooled section structure of probe.

(3) Measurement of the gas temperature of burner outlet.

A type K chromium-nickel silicon thermocouple (6 mm diameter, 10 m length) is put in a stainless steel tube to detect the gas temperature. The measuring range of thermocouple is −50 °C to 1300 °C, and its measurement accuracy is ±1 °C. The measurement end of

thermocouple is protruded from the tube, so that it can make direct contact with the flue gas. The experimental findings of Soete [28] demonstrated that while using thermocouples to measure the furnace temperature, the difference between experimental and real values did not surpass 8%. The oil gun sleeve and the monitoring port of burner are the two measuring positions, where the thermocouple is placed (see Figures 2 and 13). The thermocouple is inserted along the X direction. The zero point is the same as (1). The measurement points are set at regular intervals. Until the measured values become relatively stable, the thermocouple is left at that measurement point for 60 s, with readings recorded every 10 s. Average valves are then taken as the gas temperature at that specific point. Ignition temperature of lean coal and anthracite ranges from 754 to 1090 °C [29], while that of bituminous coal is 570 °C [30]. To facilitate the mutual comparison of different experimental conditions and determine the ignition point, this paper assumes that the ignition temperature of air-coal mixture is 750 °C. This presumption can make it easier to compare experimental data, which improves our understanding of the burner performance under various settings.
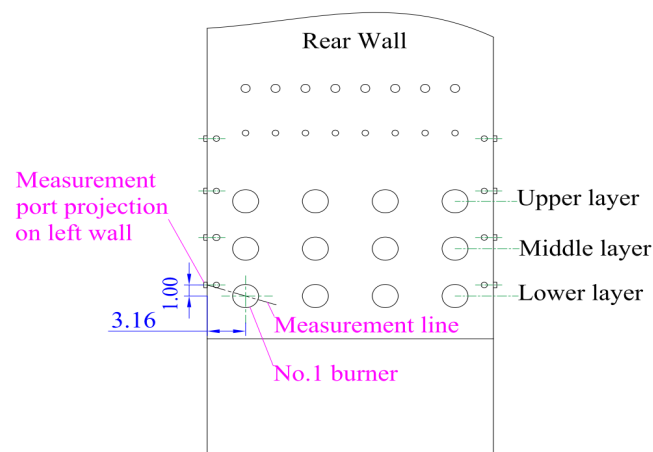
Figure 15. Position of measurement port on left wall.

(4) Measurement of furnace temperature.

During the low-load steady combustion test, the Raytek 3i plus optical pyrometer, with a measurement error of 5% [31], was used to measure the furnace temperature. The temperature was measured at the measurement ports located on the front wall, rear wall as well as side walls (see Figure 1, each port located 1.0 m higher than the burner elevation). Multiple temperature readings were taken at each port, and the average value of one port was used to determine the furnace temperature there.

4.2. Result of Situ Industrial Experiments

In order to investigate the effect of central air on the combustion characteristics of Babcock burner, experiments were conducted at three different boiler loads: 444 MW (63% rated load), 522 MW (75% rated load), and 645 MW (92% rated load), with variable central air mass flow for burner No. 2. The valve opening of burner center air was adjusted at several positions (0%, 30%, 60% and 100%) to regulate the center air mass flow. Under each operating circumstance, the flue gas temperature was concurrently measured at the burner center and burner measurement port. In addition, the gas composition and concentration in the axial and radial directions of burner center were carried out. The optimum valve opening of burner center air was also chosen by combining the results of aforementioned cold-state and hot-state testing. Furthermore, low-load steady combustion tests were conducted at boiler loads of 280 MW (40.0% rated load) and 262 MW (37.4% rated load), respectively.

The coal analysis during experiment can be seen in Table 4. With a slight difference, the dry ash-free basis volatile (V_{daf}) is 21.9%, 19.9%, 19.7%, and 18.87%, respectively. Table 5 provides the average operating parameters of boiler during the experimental period.

Table 4. Ultimate and proximate analyses of the coal used in industrial measurements.

Boiler load	Proximate analysis (wt.%)				Net heating value (kJ/kg)
	FC_{ad} [a]	A_{ad} [1]	V_{ad}	M_{ad}	
444 MW	53.10	30.28	14.90	1.72	20,667
522 MW	54.13	31.04	13.41	1.42	20,998
645 MW	53.34	32.48	13.10	1.08	20,775
280 MW&262 MW	57.08	27.66	13.28	1.98	21,160
Boiler load	Ultimate analysis (wt.%)				
	C_{ad}	H_{ad}	O_{ad} [a]	N_{ad}	S_{ad}
444 MW	57.58	2.65	5.56	0.88	1.24
522 MW	57.81	2.57	5.08	0.86	1.22
645 MW	57.26	2.70	4.47	0.87	1.14

[a] Calculated by difference. FC Fixed carbon; A ash; V volatile matter [1] air dry basis.

Table 5. Major operating parameters of boiler at different loads.

Item	444 MW	522 MW	645 MW	280 MW	262 MW
Main steam flow (t·h^{-1})	1339	1574	1945	844	790
Main steam pressure (MPa)	14.1	15.4	16.3	14.5	14.5
Main steam temperature (°C)	535	534	536	520	517
Reheat stream temperature (°C)	539	536	538	532	530
Reheat stream pressure (MPa)	1.59	2.01	2.84	1.29	1.22
Primary air temperature (°C)	110	110	119	110	110
Secondary air temperature (°C)	315	327	325	315	315
Total fuel consumption (kg·s^{-1})	56.9	68.1	75.0	32.0	29.9
Minimum temperature at denitration inlet (°C)	354	358	377	313	310

4.2.1. Measurements of Gas Temperature in the Burner Region

The central temperature distribution pattern of burner No. 2 under different rated loads is similar, as can be seen in Figure 16. This indicates that the effect of load variation on the center temperature is small. The influence of central air valve opening, however, is more dramatic. With the increase of valve opening, the temperature in burner center gradually increases, but the highest temperature does not exceed 450 °C. It means that the pulverized coal does not catch fire in the range of 0–2.4 m. When the central air is completely closed, the temperature of burner center is instead the lowest. Combined with the single-phase test (see Figure 4), it can be seen that when the central air mass flow is 0, there is a central recirculation zone at the central air duct outlet (near x/d = 0) and x/d = 1.07–1.87. In actual operation, there is no coal powder in the small recirculation zone, and that the large recirculation zone is far from the primary air outlet. Both of the two recirculation zones have no enhancement to stable combustion. More importantly, the zone of central air flow is located in the burner center. And the rotating primary air is moving with a high radial velocity at the same time (see Figure 9). These may lead to a very low coal concentration in the burner center region. As a result, it is difficult to catch fire in the center. Actually, the temperature measured in burner center depends mainly on the convective heat transfer between the unfired air and the thermocouple. A higher central air valve opening results in a faster heat transfer between them; thus, resulting in a higher temperature at the same measurement distance.
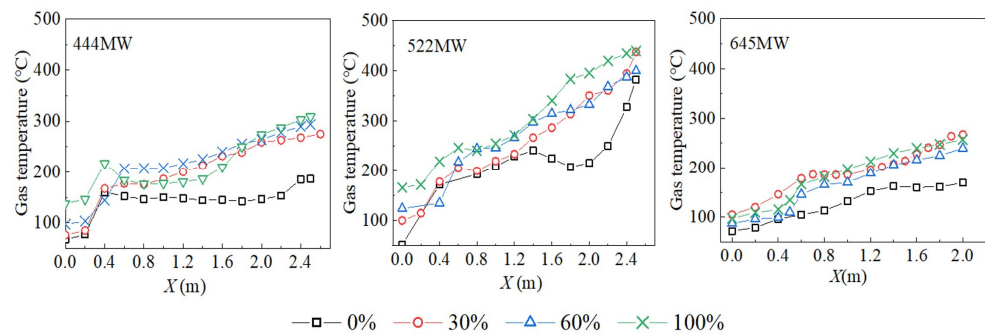
Figure 16. Temperature at the burner center under different center air valve opening.

The temperature at burner monitoring port was measured at different center air valves opening, as shown in Figure 17. It can be seen that at the same distance X, the overall temperature at this position is higher than that of burner center. The coal is already ignited near the outlet. Combined with the single-phase test results (see Figure 5), the burner port area is inside the annular recirculation zone, thus the pulverized coal can catch fire in time. In addition, with the increase of the central air valve opening, the temperature gradually decreases. It can be noted from Figures 10 and 11 that, while the central air mass flow is increased, the position of maximum axial positive velocity and the maximum tangential velocity are both closer to the burner central axis. This phenomenon is not conducive to the mixing of primary air and secondary air. Similarly, during the industrial test, the central air mass flow increased when the center air valve opening turned up. This ultimately results in delayed ignition because the pulverized coal is unable to make timely contact with the secondary air. Therefore, to ensure the stable combustion performance of burner in actual operation, a smaller central air valve opening must be chosen.
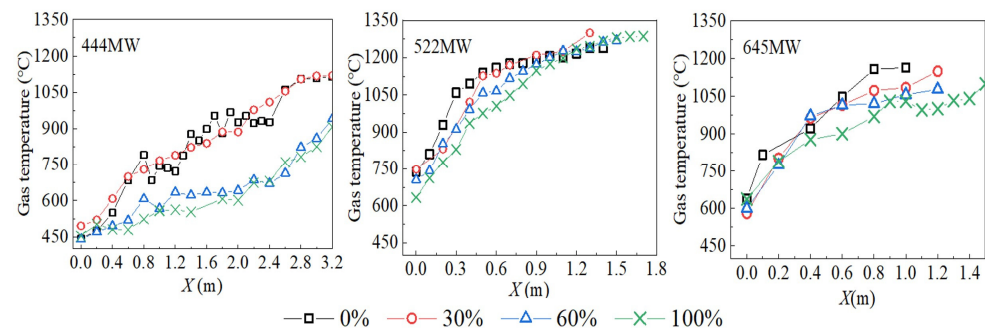
Figure 17. Temperature at the monitoring port of burner under different center air valve opening.

In order to represent the effect of central air on pulverized coal combustion more obviously, the heating rate β and the ignition position l (the distance from ignition position to primary air duct outlet) were calculated. The heating rate can be seen in Figure 18, while the ignition distance is depicted in Figure 19.

A higher heating rate is a prerequisite for the timely ignition of pulverized coal. For the parameter β, the measurement range for burner center is 0 to 2.0 m, and for monitoring port of burner is 0 to 1.2 m, where 0 m indicates the distance to the plane of primary air outlet. As can be found from Figure 16, within the range of 0 to 2.0 m at burner center, the pulverized coal does not ignite under the three loads. Therefore, β in burner center, as shown in Figure 18, is significantly lower. In contrast, at the monitoring port of burner, the pulverized coal catches fire early and therefore has a higher β. At different loads, the central air flow had no significant impact on burner center β. However, the effect of central air flow on monitoring port β is more obvious at 444 MW. The pattern presented is that while the central air flow decreases, β gradually accelerates.
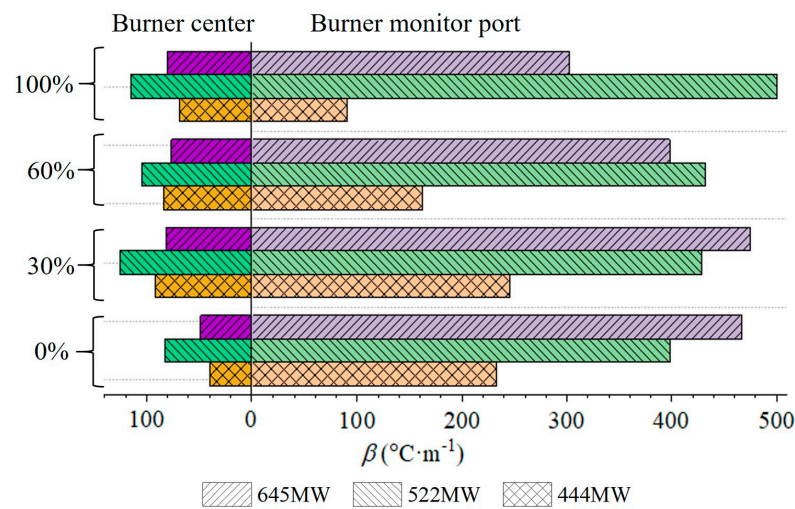
Figure 18. Heating rate at different valve opening of central air.

At all loads, the coal located in burner center is not catching fire. As a result, all *l* in Figure 19 can be only found in the monitoring port area. It can be seen from Figure 19 that at 444 MW, *l* is only 0.8 m at 0% and 30% of central air valve opening, but it is more over 2.5 m at 60% and 100%. When the central air valve is between 0% and 30% at 522 MW, the coal ignites close to the primary air outlet; between 60% and 100%, *l* is around 0.1 m. At all four valves opening for 645 MW, the coal burns within 0–0.15 m. It can be concluded that the variation of central air flow has a significant effect on *l* at 444 MW. The central air valve opening for sudden change of *l* under 444 MW is 60%. The ignition distance *l* is related to the heating rate β. Figure 18 shows that at 444 MW, the heating rate significantly drops at 60% of the central air valve opening, resulting in a longer ignition distance.
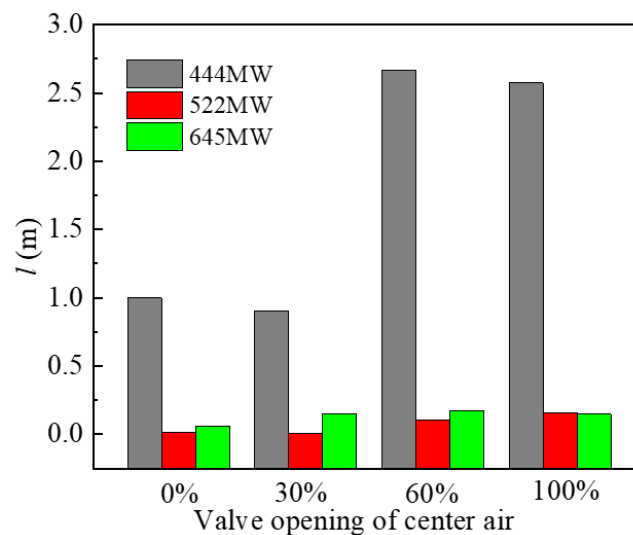
Figure 19. Ignition distance with different valve opening of center air.

According to the research of *l* and β, choosing a lower central air flow (30% valve opening) is essential, if the boiler is working under a low load. As a result, the pulverized coal starts burning earlier at the burner outlet, enhancing efficiency and optimizing the combustion process.

4.2.2. Measurements of Gas Species Concentrations in the Burner Region

The central air valve opening was adjusted to 30% for all burners in the lower rear wall. On burner No. 2 (see Figure 13), measurements of the flue gas components and

concentrations were carried out at loads of 444 MW, 522 MW and 645 MW, respectively. The flue gas components and concentrations of burner No. 1 were measured simultaneously in a radial direction from the left wall measurement port (see Figure 15). The flue gas concentrations (O_2, CO, and NO_x), measured through the burner center and the measuring port on left wall, are displayed in Figure 20.

The distribution of O_2, CO, NO_x at the burner center is included in Figure 20. As can be indicated, for any load in the range of 0 to 1.5 m, the O_2 concentration is roughly equal to the oxygen content of air and does not fluctuate significantly. This shows that there is no coal combustion in this range. The result is consistent with the temperature measurement in Figure 16. Also, the CO content is extremely low, ranging between 0–1.5 m, with a maximum concentration of no more than 25 ppm. It further indicates that the pulverized coal is not burning. While the measurement distance is increased, the NO_x content gradually increases. However, because the pulverized coal is not burning, the difference in NO_x content is minimal for all loads. The NO_x level was around 350 mg/m^3 (6% O_2) when 1.5 m away from the outlet of primary air duct.
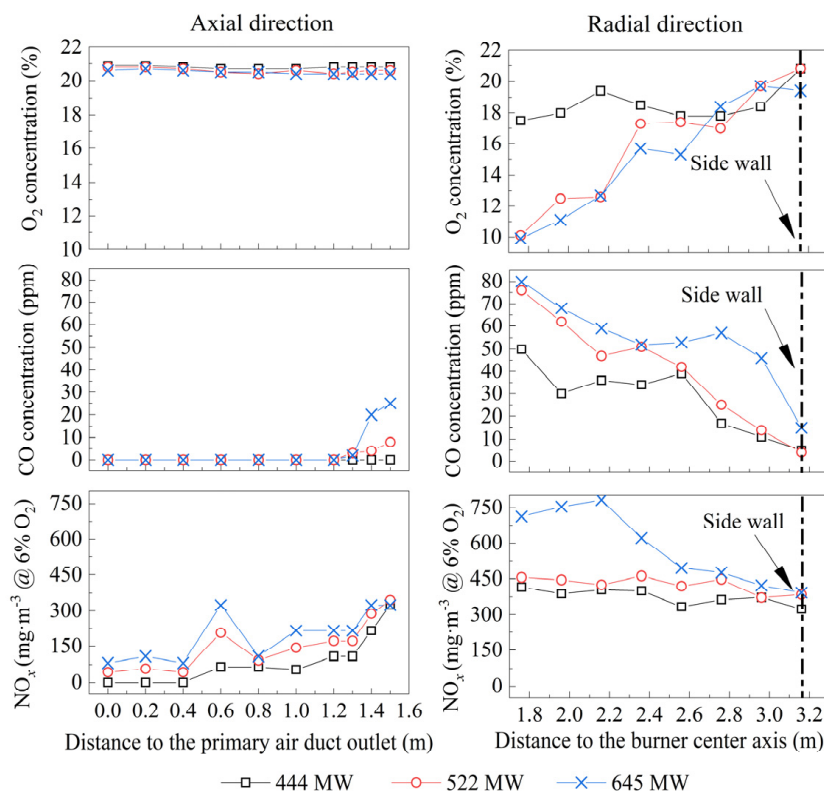
Figure 20. Gas components and concentrations in the axial and radial directions of burner.

The distribution of O_2, CO, NO_x obtained from the measurement port on left wall is also included in Figure 20. For different loads of 444 MW, 522 MW and 645 MW, the corresponding O_2 concentrations are 20.8%, 20.8% and 19.4%, respectively. As the measurement position approaching to the burner centerline, the O_2 concentration tends to steadily drop. The O_2 concentration decreases to around 10% at both the 522 MW and 645 MW, in a distance of 1.76 m. At 444 MW, the O_2 concentration falls off less than it does at the other two loads, but it still remains much higher. Similarly, the maximum concentration of CO is no more than 80 ppm for the three loads. Overall, the oxygen concentration in the radial direction is relatively high, further indicates the inadequate combustion of coal. The NO_x concentrations at 444 MW and 522 MW are roughly 400 mg/m^3 (O_2 = 6.0%) and 450 mg/m^3 (O_2 = 6.0%), respectively, with not much of a difference between them. NO_x from coal combustion is mainly fuel-based NO_x. At high load, the furnace temperature is

high, making coal easier to ignite. Thus, the NO_x concentration at 645 MW is around 400 to 800 mg/m^3 (O_2 = 6.0%), with higher levels.

4.2.3. Boiler Low Load Operation Experiment

In the context of flexible peaking, boilers need to have the ability to operate at low loads for long periods time. When the boiler load is below the limit of stable combustion, oil injection is necessary to achieve stable combustion and prevent flameout. However, Zhang et al. [32] pointed out that a long-term oil injection operation has certain negative effects on the dust removal electrode and desulfurization slurry. Therefore, it is critical to improve the minimum low-load stable combustion capacity without oil support.

The low load test was carried out at 280 MW (40.0% rated load) and 262 MW (37.4% rated load), respectively. The coal analysis during the test can be seen in Table 4, and the main operating parameters of boiler are shown in Table 5. To keep the central oil gun cool during the actual operation, a specific amount of central air must be retained. Therefore, the central air valves opening of all burners was adjusted to 30% for the low-load stable combustion test.

The unit performs load reduction with a constant pressure operation. The average load reduction rate between 350 MW and 280 MW is 0.67 MW/min. The burner arrangement can be seen in Figure 1. At 280 MW, the upper layer of the front wall and rear wall acted as the non-operating burners, while the lower and middle layers served as the operational burners. During 280 MW test, the negative pressure in the furnace chamber maintained steady and none of the heating surfaces overheated. The stable operation lasted for 60 min continuously. Then, in order to further investigate the boiler's capabilities for low load operation, the middle layer of the front wall was turned off based on 280 MW. The boiler load was decreased to 262 MW with an average load reduction rate of 1.2 MW/min and stable operation for 75 min. Also, during 262 MW, the parameters were accord with the demands of design.

The furnace temperature was measured from the measurement ports mentioned in Section 4.1 (4). The position of measurement ports is described in Figure 1. The measured furnace temperature is given in Figure 21. The lowest temperature, at 280 MW, is 936 °C, as shown in Figure 21a. The total temperature is steady, with an average temperature of 1112.0 °C in the burner area. Similar to this, at 262 MW, the average temperature is 1056.1 °C, and the lowest temperature is 976 °C, as shown in Figure 21b. The average temperature of 262 MW is a little lower than that of 280 MW. For stable combustion, a higher furnace temperature must be maintained. The average temperature of the main combustion zone is greater than 936 °C at both loads, which is 186 °C higher than the ignition point of lean coal (750 °C). According to the furnace temperature, this 700 MW boiler can successfully operate steadily at rated load 37.4%, with 30% valves opening of all burner central air. The fuel for this boiler is a mixture of lean coal and bituminous coal. According to the categorization based on power coal, lean coal typically has a dry ash-free volatile matter (V_{daf}) content ranging from 10% to 20%. It belongs to a coal variety with relatively poor reactivity, with an ignition temperature of approximately 750 °C. The V_{daf} content of bituminous coal ranges from 20% to 28%, with an ignition temperature of approximately 570 °C [30]. On the other hand, lignite coal, with a V_{daf} content of 40% to 50% or even higher, is prone to spontaneous combustion. Blending a certain proportion of bituminous coal or lignite into lean coal can enhance the combustion performance of lean coal-fired boilers. As a result, there is a promising prospect of reducing the minimum stable combustion rated load without oil support of the boiler to 30%, thereby further enhancing its peak load regulation capability.

(a)

Height: 19.80m

	1085°C		1223°C
985°C	Rear·wall	-	1105°C
1151°C	Front·wall	936°C	1098°C
	1239°C		1046°C

Height: 21.93m

Height: 24.05m

	1154°C		1159°C
1095°C 1197°C	Rear·wall		
1035°C 1140°C	Front·wall		
	1181°C		1098°C

Height: 26.18m

Height: 28.30m

	-		-
1197°C	Rear·wall	1170°C	
1140°C	Front·wall	1037°C	
	1173°C		1046°C

Height: 30.43m

(b)

Height: 19.80m

	1072°C		1196°C
976°C	Rear·wall	-	1103°C
1102°C	Front·wall	992°C	1052°C
	1267°C		1051°C

Height: 21.93m

Height: 24.05m

	1139°C		1138°C
1103°C 1184°C	Rear·wall		
1026°C 1130°C	Front·wall		
	1181°C		1098°C

Height: 26.18m

Height: 28.30m

	-		-
1184°C	Rear·wall	1154°C	
1130°C	Front·wall	1028°C	
	1123°C		1055°C

Height: 30.43m

Figure 21. The furnace chamber temperature: (**a**) 280 MW, (**b**) 262 MW.

5. Discussion

Flexible peak regulation of lean coal-fired boilers has always been a major problem. In this paper, the single-phase flow characteristics of Germany Babcock burner are studied in detail from laboratory tests. The industrial test was carried out on a lean-coal fired boiler with this type of burners, and the combustion characteristics of the burner were obtained. Combining the above single-phase cold test and industrial test results, the optimal burner operating parameters were obtained (30% central air valves opening). Furthermore, a low-load stable combustion test was conducted using the results of the work mentioned above. The experiment successfully reduced the minimum stable combustion load without oil injection to 262 MW (37.4% rated load). The above work provides experimental data for the following numerical simulation analysis, and further serves as a guide for the flexible peak regulation of lean coal-fired boilers.

6. Conclusions

The impact of central air on the flow and combustion characteristics of a Babcock burner was studied using laboratory and industrial tests. Also, a boiler low-load steady combustion test was performed at the optimal central air flow. These were results:

(1) After x/d = 0.5, the axial and radial velocities at burner center decreased while the center air mass flow decreased from 130% to 0%. The position of maximum axial positive velocity and the maximum tangential velocity were both gradually moved away from the burner center. The optimal central air mass flow of this burner is between 0% and 30%.

(2) The temperature distribution pattern at burner outlet is consistent at 444 MW, 522 MW and 645 MW. That was, the temperature of central area was much lower than that of secondary air area, and the ignition of burner center was relatively late. At the same load, the temperature of center region gradually increased with the center air valve opening from 0% to 100%. The temperature of secondary air zone, on the other hand, gradually declined, but the pulverized coal still managed to catch fire in time. The central air mass flow had a major influence on the ignition distance at 444 MW, and 60% of the valve opening corresponded to a sharp rise in ignition distance. The optimal central air valve opening of this burner is between 0% and 30%.

(3) In the range of 0–1.5 m from the primary air outlet, the O_2 concentration kept approaching 21% with increasing boiler load; in contrast, the CO and NO_x concentrations gradually increased. The pulverized coal in the burner center had not been ignited. The result taken from the sidewall indicated that the O_2 concentration was lower along the center axis of burner, while the concentration of CO was higher in that same area. When the boiler load is decreased, the concentration of O_2 increased significantly.

(4) While the valves opening of burners central air was 30%, the boiler minimum stable combustion rated load without oil support could be reduce to 37.4%. The negative pressure

of furnace chamber remained stable during 37.4% rated load, and the main steam pressure and temperature fulfilled the design requirements. The lowest temperature recorded in the main combustion zone was 936 °C, with an average temperature of 1056.1 °C.

Author Contributions: Conceptualization, C.H. and Z.L.; methodology, Z.L. and C.H.; software, C.H.; validation, C.H., Y.W., Y.L. and H.L.; formal analysis, C.H.; investigation, Z.L. and C.H.; resources, Z.L. and Z.C.; data curation, C.H.; writing—original draft preparation, C.H.; writing—review and editing, Z.L.; visualization, C.H. and Y.W.; supervision, Z.L.; project administration, Z.L.; funding acquisition, Z.L. All authors have read and agreed to the published version of the manuscript.

Data Availability Statement: All relevant data are within the paper.

Conflicts of Interest: The authors declare no conflict of interest.

References

1. Miao, Y.C.; Liu, S.H.; Zheng, Y.J; Wang, S.; Chen, B.; Zheng, H.; Zhao, J. Numerical study of the effects of local atmospheric circulations on a pollution event over Beijing-Tianjin-Hebei, China. *J. Environ. Sci.* **2015**, *30*, 9–20. [CrossRef]
2. Hu, H.; Yang, Q.; Lu, X.; Wang, W.; Wang, S.; Fan, M. Air pollution and control in different areas of China. *Crit. Rev. Environ. Sci. Technol.* **2010**, *40*, 452–518. [CrossRef]
3. Thomas, R.A.; Hawkins, E.; Philip, D.J. CO_2, the greenhouse effect and global warming: From the pioneering work of Arrhenius and Callendar to today's Earth System Models. *Endeavour* **2016**, *40*, 178–187.
4. National Energy Administrator. January to February 2023 National Electricity Industry Statistics. Available online: https://www.nea.gov.cn/2023-03/21/c_1310704448.htm (accessed on 20 May 2023).
5. Verleysen, K.; Coppitters, D.; Parente, A.; De Paepe, W.; Contino, F. How can power-to-ammonia be robust? Optimization of an ammonia synthesis plant powered by a wind turbine considering operational uncertainties. *Fuel* **2020**, *266*, 117049. [CrossRef]
6. Bai, X.F.; Ding, H.; Lian, J.J.; Ma, D.; Yang, X.; Sun, N.; Xue, W.; Chang, Y. Coal production in China: Past, present, and future projections. *Int. Geol. Rev.* **2018**, *60*, 535–547. [CrossRef]
7. Yin, C.G.; Rosendahl, L.; Condra, T. Further study of the gas temperature deviation in large-scale tangentially coal-fired boilers. *Fuel.* **2003**, *82*, 1127–1137. [CrossRef]
8. Song, M.H.; Huang, Y.; Huang, Q. Discussion on low-load stable combustion technology of swirl pulverized-coal burner. *Proc. CSEE* **2021**, *41*, 4552–4566.
9. Zeng, L.Y.; Li, Z.Q.; Zhao, G.B.; Shen, S.; Zhang, F. Effect of the vane angle for outer secondary air on the flow and combustion characteristics and NO_x emissions of the low-NO_x axial-swirl coal burner. *Numer. Heat Transf. Part A* **2011**, *59*, 43–57. [CrossRef]
10. You, C.F.; Zhou, Y. Effect of operation parameters on the slagging near swirl coal burner throat. *Energy Fuels* **2006**, *20*, 1855–1861. [CrossRef]
11. Ochi, K.; Kiyama, K.; Yoshizako, H.; Okazaki, H.; Taniguchi, M. Latest low-NO_x combustion technology for pulverized-coal-fired boilers. *Hitachi Rev.* **2009**, *58*, 187–193.
12. Liu, J.Q.; Sun, B.M.; Zhang, G.C. Numerical simulation and optimization on stable combustion of a 1000 MW ultra supercritical unit swirl combustion boiler. *Proc. CSEE* **2012**, *08*, 19–27.
13. Wang, L.; Li, Z.Q.; Hao, J.B.; Song, Z. Effct of central air on the performance of the swirl burner. *Chin. J. Mech. Eng.* **2000**, *06*, 63–67. [CrossRef]
14. Wang, L.; Wu, S.H.; Li, Z.Q. The effects of cenrtal air on combustion of the radial bias combustion swirl burner. *Power Eng.* **2000**, *20*, 615–619.
15. Lu, H.; Liu, H.F.; Li, W.F.; Xu, J.L. Bubble formation in an annular granular jet dispersed by a central air round jet. *AIChE J.* **2013**, *59*, 1882–1893. [CrossRef]
16. Huang, L.Y.; Liu, C.C.; Deng, T.D.; Jiang, H.; Wu, P. Experimental investigation on the influence of central airfow on swirl combustion stability and fame shape. *J. Therm. Anal. Calorim.* **2021**, *144*, 503–514. [CrossRef]
17. Chen, Z.C.; Li, Z.Q.; Zhu, Q.Y.; Jing, J. Gas/particle flow and combustion characteristics and NO_x emissions of a new swirl coal burner. *Energy* **2011**, *36*, 709–723. [CrossRef]
18. Al-Halbouni, A.; Giese, A.; Tali, E.; Leicher, J.; Albus, R.; Görner, K. Combustor concept for industrial gas turbines with single digit NO_x and CO emission values. *Energy Procedia* **2017**, *120*, 134–139. [CrossRef]
19. Han, J.D.; Zhu, L.B.; Lu, Y.P.; Mu, Y.; Mustafa, A.; Ge, Y. Numerical simulation of combustion in 35 t/h industrial pulverized coal furnace with burners arranged on front wall. *Processes* **2020**, *8*, 1272. [CrossRef]
20. Xie, B.; Zhang, G.C. Effect of center wind on combustion characteristics of HT-NR3 swirl burner. *Therm. Power Gener.* **2015**, *44*, 35–40+45.
21. Marcel, R.; Gerd, O.; Klaus, G. Improving the load flexibility of coal-fired power plants by the integration of a thermal energy storage. *Appl. Energy* **2019**, *236*, 607–621.

22. Martin, K.; Michal, K. Control of a boiler-turbine unit using MPC-based reference governors. *Appl Therm Eng.* **2017**, *110*, 1437–1447.
23. Li, Z.Q.; Kuang, M.; Zhu, Q.Y. Aerodynamic characteristics within a cold small scale model for a down-fired 350 MWe utility boiler applying a multiple injection and multiple-staging technology: Effect of the staged-air declination angle. *Exp. Therm. Fluid. Sci.* **2012**, *38*, 184–194. [CrossRef]
24. Chen, Z.C.; Li, Z.Q.; Jing, J.P.; Chen, L.; Wu, S.; Yao, Y. Study on flow fields of centrally fuel rich swirl burner and its applications. *Korean J. Chem. Eng.* **2009**, *26*, 1186–1193. [CrossRef]
25. Mueller, U.R. On the accuracy of turbulence measurements with inclined hot-wires. *J. Fluid. Mech.* **1982**, *119*, 155–172. [CrossRef]
26. Jing, J.P.; Li, Z.Q.; Zhu, Q.Y.; Chen, Z.; Ren, F. Influence of primary air ratio on flow and combustion characteristics and NO_x emissions of a new swirl coal burner. *Energy* **2011**, *36*, 1206–1213. [CrossRef]
27. Li, S.; Li, Z.Q.; Jiang, B.K.; Chen, Z.; Zhang, X. Effect of secondary air mass flow rate on the airflow and combustion characteristics and NO_x formation of the low-volatile coal-fired swirl burner. *Asia Pac. J. Chem. Eng.* **2015**, *10*, 858–875. [CrossRef]
28. De Soete, G.G. Measurement of flame temperature with a multi-element thermocouple. *J. Energy Inst.* **1981**, *54*, 113–116.
29. Xie, J.Y.; Chen, H.W. Distribution of ignition temperature and ignition heat of power coal in China. *CIESC J.* **2015**, *66*, 4170–4176.
30. Guo, L.; Zhai, M.; Wang, Z.; Zhang, Y.; Dong, P. Comparison of bituminous coal and lignite during combustion: Combustion performance, coking and slagging characteristics. *J. Energy Inst.* **2019**, *92*, 802–812. [CrossRef]
31. Li, X.G.; Zeng, L.Y.; Zhang, X.; Fang, N.; Song, M.; Chen, Z.; Li, Z. Effects of the fuel-lean coal/air flow damper opening on combustion, energy conversion and emissions in a supercritical down-fired boiler. *Fuel* **2021**, *292*, 120319. [CrossRef]
32. Zhang, S.Q.; Chen, L.; Liu, Z.Y. Discussion on key problems of depth peak adjustment for large coal-fired boilers. *South. Energy Constr.* **2022**, *9*, 16–28.